Polymer Journal (2019) 51:721–730
https://doi.org/10.1038/s41428-019-0192-5

FOCUS REVIEW

Microstructured rubber and its wettability

Yuji Hirai[1] · Hiroyuki Mayama[2] · Riku Tamura[1] · Yasutaka Matsuo[3] · Takahiro Okamatsu[4] · Toshihiko Arita[5] · Masatsugu Shimomura[1]

Received: 31 January 2019 / Revised: 13 March 2019 / Accepted: 17 March 2019 / Published online: 22 April 2019

Abstract

Microstructured surfaces have been attracting a considerable amount of attention for many practical applications, such as superhydrophobic materials. The key issue in everyday applications of superhydrophobic materials based on microstructured surfaces is their durability because most microstructures are prepared with stiff and fragile materials and are easily broken mechanically. In this study, we focused on vulcanized rubber as a flexible and durable hydrophobic material for the fabrication of microstructured surfaces. Superhydrophobic spiky microstructures were simply prepared from vulcanized rubber by using a silicon micromold and compact hot-press equipment. Owing to the elasticity of the vulcanized rubber, the spike-array arrangements on the rubber surface were reversibly deformed by repeated stretching without destruction of the spiky microstructures. Surface wettability was affected by the spike-array arrangements, which can be controlled by stretching concomitantly with the degree of elongation. This phenomenon was theoretically explained by the wettability transition from a Cassie–Baxter to a Wenzel state considering water penetration into the gaps among the spiky microstructures. The results indicated that microstructured vulcanized rubber surfaces can be applicable to a wide variety of fields because of the superior functions derived from their microstructures.

Introduction

In recent years, superhydrophobic microstructured surfaces, for example, lotus leaves [1], moth eyes [2], and so on [3–6], have become a topic of much interest based on their potential functions, such as self-cleaning [7–9], water manipulation [10–13], water separation [14, 15], and so on [16, 17]. There are two famous equations expressing superhydrophobicity: Wenzel's equation [18] and the Cassie–Baxter equation [19]. Wenzel's equation (1), applicable to wetted rough surfaces, is as follows:

$$\cos\theta_w = R\cos\theta, \tag{1}$$

where θ_w is the water contact angle (WCA) on a wetted rough surface, θ is the WCA on a flat material surface, and R is the roughness factor defined as the ratio of the true and apparent surfaces of the material. This equation simply indicated that WCAs are enhanced by surface roughness. Accordingly, fractal surfaces consisting of hydrophobic materials show remarkably large WCAs [20]. When a surface consists of two or more materials, the Cassie–Baxter equation (2) is adopted:

$$\cos\theta_c = f_1\cos\theta_1 + f_2\cos\theta_2, \tag{2}$$

Here, θ_c is the WCA of the Cassie–Baxter state, f_1 and f_2 are fractions of each surface composing the material, and θ_1 and θ_2 are the WCAs on flat surfaces of those materials. In most cases, for a superhydrophobic surface having a large

✉ Yuji Hirai
y-hirai@photon.chitose.ac.jp

[1] Department of Applied Chemistry and Bioscience, Chitose Institute of Science and Technology (CIST), Bibi758-65, Chitose 066-8655, Japan

[2] Department of Chemistry, Asahikawa Medical University, E2-1-1-1, Midorigaoka, Asahikawa 078-8510, Japan

[3] Nanotechnology Research Center, Research Institute for Electronic Science (RIES), Hokkaido University, N21W10, Kita-ku, Sapporo 011-0021, Japan

[4] The Yokohama Rubber Co., Ltd, 2-1, Oiwake, Hiratsuka 254-8601, Japan

[5] Institute of Multidisciplinary Research for Advanced Materials (IMRAM), Tohoku University, 2-1-1, Katahira, Sendai 980-8577, Japan

surface area, one material is air (the WCA of air is regarded as 180°), and the Cassie–Baxter equation can be altered as shown below (3):

$$\cos\theta_c = -1 + f_1(\cos\theta_1 + 1). \quad (3)$$

This equation indicates that a reduction in the water contact area (f_1) is important for superhydrophobic surfaces and that, in many instances, spiky nano- and microstructures are prepared from various materials [21]. According to the equations, how to prepare a large surface area from hydrophobic materials is important for the preparation of superhydrophobic materials, and a large number of papers have been published [22–26].

As mentioned above, there have been many reports on artificial superhydrophobic surfaces; however, a number of unresolved problems remain. First, superhydrophobic materials are usually prepared from stiff and fragile materials, so it is difficult to apply them to daily use, as the surface nano- and microstructures are easily destroyed by contact, resulting in a loss of superhydrophobicity. Therefore, poly(dimethyl siloxane), which is a typical soft hydrophobic material, has been used due to its easy handling, processability, transparency, and flexibility [27–29]. However, although this silicone elastomer is a useful material, it is relatively expensive for daily uses or in paints and is also rather brittle without composite materials. We therefore have focused on vulcanized rubber, which is a common durable material used in tires, rubber bands, and so on [30–32]. Furthermore, the characteristics of vulcanized rubber can be adjusted through changes to its compositions by the inclusion of carbon black, silica, sulfur, and so on, and various compositions have already been developed for various purposes over its long history. Here, we first describe how to prepare vulcanized rubber microstructures as simply as possible and thereafter demonstrate their surface functions with a focus on the wettability generated by the microstructures [33]. Furthermore, we attempt to understand the changes in the wettability of the vulcanized rubber microstructures by theoretical analysis.

Materials and methods/experimental procedure

The unvulcanized rubber compositions used in this experiment are listed in Table 1. The unvulcanized rubbers were placed on single-crystalline silicon molds with finely patterned microstructures prepared by conventional photolithographic techniques [34, 35], then compressed at 5 MPa, and finally heated at 180 °C for 10 min (H300-15 Compact Hot-Press System, AS ONE Corporation, Japan) to vulcanize the material. After that, the vulcanized rubbers were simply removed from the silicon molds and observed using laser microscopy (OLS4000, Olympus Corporation, Japan) and a field-emission scanning electron microscope (FE-SEM, 5.00 kV, 80 µA, JSM-7800F, JEOL, Japan) after sputtering with Pt to a thickness of approximately 6 nm (30 mA, 80 s, JEC-3000FC, JEOL, Japan).

Table 1 Composition of the rubber compounds used in this research

	Rubber 1	Rubber 2	SBR
Natural rubber	100	100	0
SBR	0	0	100
Silica	0	0	70
Carbon black	35	70	5
Coupling agent	0	0	5.5
Sulfur	3.5	3.5	2.5
Accelerator	2.5	2.5	3
Oil	5	5	7
Total	146	181	193

"phr" means "per hundred rubber" or parts by weight per 100 parts versus the weight of natural rubber

SBR styrene-butadiene rubber

Water contact angles were measured using a WCA analyzer (FAMAS, Drop Master, Kyowa Interface Science, Japan) with 1.5 or 5 µL ultrapure water droplets, and the behavior of 5 µL water droplets dropped from a height of 2 cm onto the pillared vulcanized rubber surface with different degrees of elongation was recorded by a high-speed camera (EXILIM, EX- FH20, CASIO, Japan) at a frame rate of 1200 fps.

Results and discussions

Surface observations of the vulcanized rubber microstructures

Figure 1a, b shows FE-SEM images of the silicon mold used in this research. Hexagonally arranged tapered micropores (surface diameter of ca. 6.1 µm, bottom diameter of ca. 2.5 µm, and a depth of ca. 6.3 µm) are shown. Figure 1c–e shows FE-SEM images of the vulcanized rubber surfaces prepared by using a silicon mold with tapered micropores. Spiky vulcanized rubber microstructure arrays prepared from the three types of vulcanized rubber listed in Table 1 were successfully formed on the surface. This result suggests that the rubber composition did not have a significant effect on the structural transfer, as the compositions used in this experiment are generally used in tires and were not designed specifically for this research. Therefore, it is possible to obtain vulcanized rubber microstructures with a wide range of compositions.

Detailed FE-SEM observations revealed that the sides of the spikes were jagged, reflecting the shape of the silicon mold, while the tops of the spikes were smooth. According

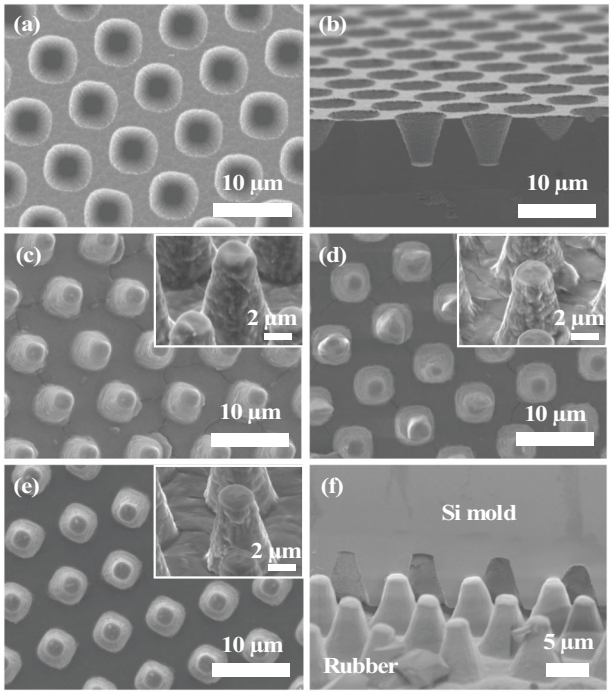

Fig. 1 Field-emission scanning electron microscope (FE-SEM) images of the silicon mold and the microstructured vulcanized rubber surfaces. **a** Top and **b** cross-sectional view of the silicon mold. Spiky vulcanized rubber structures prepared from the **c** Rubber 1, **d** Rubber 2, and **e** styrene-butadiene rubber (SBR) compounds listed in Table 1. **f** Cross-sectional view of a split sample before removal of the vulcanized rubber from the silicon mold

to the FE-SEM image shown in Fig. 1f, a transverse sample of the silicon mold and vulcanized rubber before their separation, the vulcanized rubber almost fully filled the mold micropores, although there was a little space between the bottom of the mold micropores and the vulcanized rubber. We speculated that this space was caused by compressed air and that it is the reason why the tops of the spikes were smooth and enabled easy removal of the vulcanized rubber from the silicon mold without the use of release agents (wettability differences were also important for easy peeling of the hydrophobic vulcanized rubber off the hydrophilic silicon mold with oxide surface layers). This result indicates that the formation of vulcanized rubber microstructures is feasible, but we should be somewhat concerned about the existence of trapped air that inhibits exact structure transfer from the mold to the rubber surface, although the trapped compressed air might also aid in easy removal.

Surface wettability and pattern rearrangement of the spiky vulcanized rubber by stretching

We successfully prepared vulcanized rubber microstructures with the intention of enhancing surface wettability. Before WCA measurements of the spiky vulcanized rubber surfaces, the WCAs on flat rubber surfaces composed of Rubber 1 (Table 1) were measured before and after vulcanization. The WCAs on the flat rubber surfaces were ca. 106° regardless of vulcanization, indicating that the vulcanization process did not affect surface wettability. However, the WCAs on the flat rubber surfaces were slightly higher than those on a natural rubber surface (ca. 90°–100°) [31]. This difference may have been caused by surface roughness generated by the addition of carbon black or silica. The vulcanized rubber surfaces maintained their hydrophobicity after the vulcanization process, and the WCAs on the spiky vulcanized rubber surfaces were measured with 1.5 μL of ultrapure water. As a result, the WCAs on the surfaces were ca. 158°, indicating that the spiky vulcanized rubber surfaces showed superhydrophobicity.

We inferred the state of a water droplet on the spiky rubber surface using Wenzel's and the Cassie–Baxter equation. According to Wenzel's equation (1), with a WCA on a flat vulcanized rubber surface of 106° and an R of 2.57, as measured using a laser microscope, the theoretical value of the WCA on the spiky vulcanized rubber surface was 121°, which differs significantly from the experimental value. On the other hand, the theoretical WCAs on spiky vulcanized rubber surfaces were 161° based on the Cassie–Baxter equation with a vulcanized rubber fraction f of 0.077, which was calculated as a water droplet on the top of the 2.55 μm diameter spikes, and a hexagonally arranged spike periodicity of 8.73 μm. To compare the theoretical WCAs obtained by the Cassie–Baxter equation and the experimental value, spiky vulcanized rubber surfaces were assessed in the Cassie–Baxter state.

One of the characteristics of vulcanized rubber is its elasticity. We examined structural and WCA changes induced by stretching the microstructured vulcanized rubber. Here, we chose Rubber 1, which is softest vulcanized rubber among the compounds used in this research. In this experiment, the spikes were arranged hexagonally; therefore, the surface had six-fold symmetry belonging to *p6m* in the plane crystallographic group, and there are two elongation directions, (1, 1) and (1, 0), to the equilateral triangle of the basic grid. Figure 2a–h shows three-dimensional (3D) laser microscope images taken before and after stretching the microstructured vulcanized rubber. When the microstructured vulcanized rubber was stretched in the (1, 1) direction (Fig. 2a–d), the spike arrangement changed from hexagonal to a linear pattern, and in the case of the (1, 0) direction, the spike arrangement changed to a slanted linear pattern (Fig. 2e–h). This arrangement difference was caused by deformation of underlying parts of the spikes. In the case of the (1, 1) elongation direction, the deformations were not affected by the spike arrangement because the arrangement had already been transformed before deformation of the

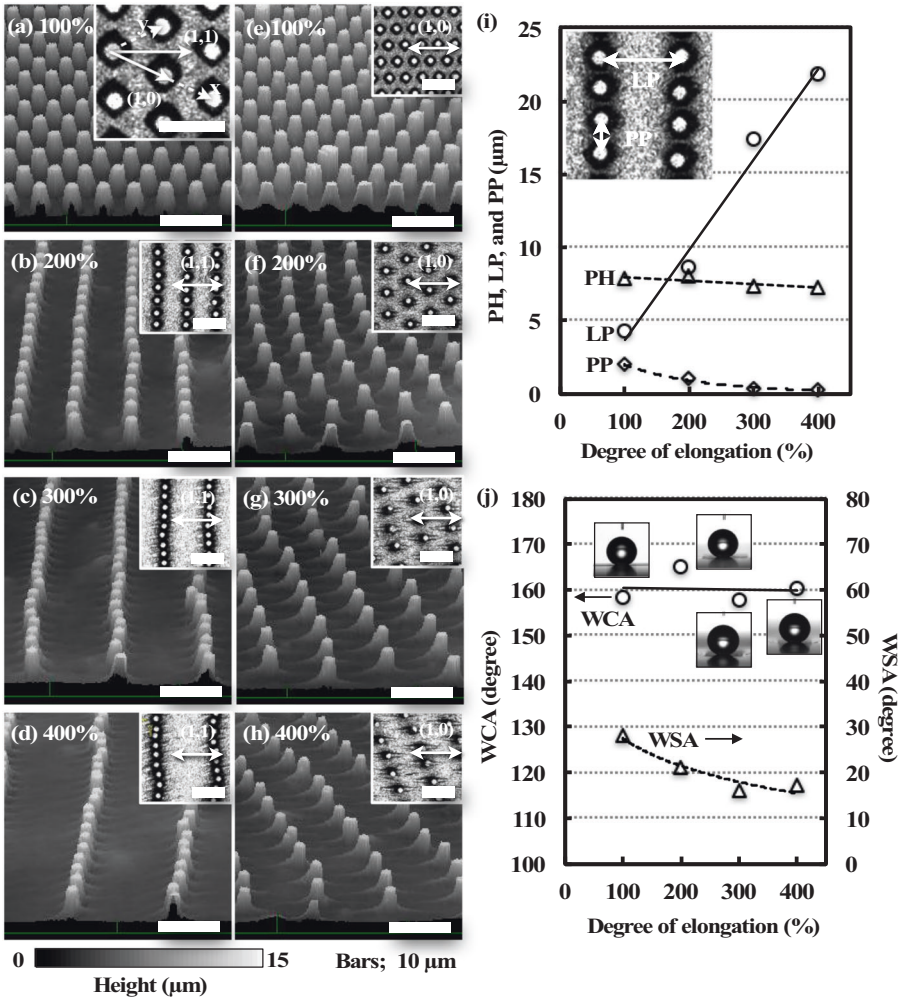

Fig. 2 Laser microscope images and graphs of spiky vulcanized rubber surfaces with different degrees of elongation. Laser microscope three-dimensional (3D) images of spiky vulcanized rubber surfaces elongated in the **a–d** (1, 1) and **e–h** (1, 0) directions. Inserted images are the top views of each surface. **i** Graph of changes in structural parameters induced by stretching. PH, LP, and PP represent spike period, line period, and spike height, respectively. Inserted images indicate the LP and PP. **j** Graph of water contact angle (WCAs) and water sliding angles (WSAs). Inserted images show photographs of a 1.5 μL water droplet on the spiky vulcanized rubber surface for each degree of elongation

underlying parts of the spikes. In the case of the (1, 0) elongation direction, once periods of spikes were elongated (Fig. 2f), vertical spike periods to the elongation directions were decreased (Fig. 2g, h). At this moment, pointed ellipse-shaped underlying parts interfered with each other, and line patterns were slanted to escape stress. Figure 2i shows graphs of the changes in the structural parameters by elongation in the (1, 1) direction. In Fig. 2i, LP represents the line period, which is the width between the newly created lines by stretching; PP represents the pillar (spike) period of the compression of distance induced by elongation; and PH represents the pillar (spike) height. According to the graph, changes in the LP were proportional to the degree of elongation, and those in the PP were inversely proportional to the degree of elongation. However, although the PH seemed to decrease slightly, in comparison to the other structural parameters, PH was relatively unchanged. In this vulcanized rubber, the spiky structures seemed to be formed on the surface of the vulcanized rubber sheet so that when the vulcanized rubber was elongated, the bottom of the vulcanized rubber sheet stretched initially and the spiky structures were not affected. This fact indicates that we can transform the spike arrangement by stretching without destroying or deforming the spiky structures. Figure 2j shows the graph of changes in the WCAs and water sliding angles (WSAs) induced by stretching. The WCAs were not changed, as the rubber fraction f was also not changed significantly; however, the WSAs decreased slightly with increases in the degree of elongation. Unfortunately, the linearly patterned spiky vulcanized rubber surfaces did not show any water sliding directional anisotropy, as these surfaces were too water repellent to affect the direction of water sliding. According to these results, vulcanized rubber surfaces can realize superhydrophobicity, and their microstructure arrangements can be deformed without destroying the microstructures. Furthermore, although spiky vulcanized rubber surfaces were too water repellent, the results suggested the possibility of wettability control through stretching of the vulcanized rubber microstructure arrangement.

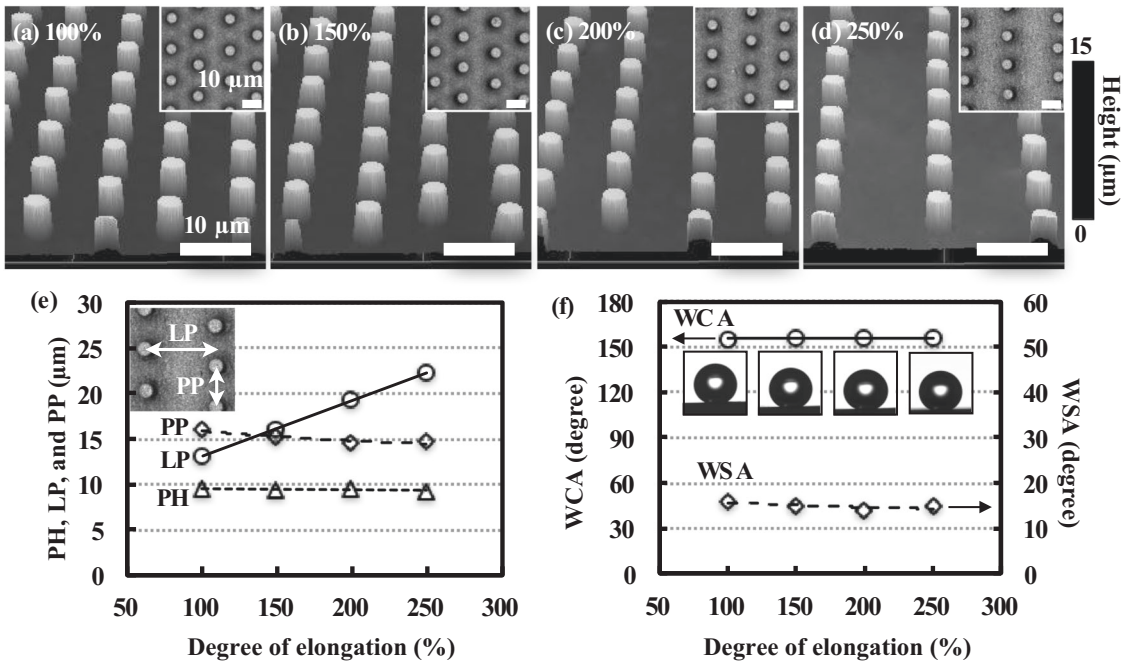

Fig. 3 Laser microscope images and graphs of vulcanized rubber micropillar surfaces with different degrees of elongation. The elongation direction was (1, 1). **a–d** Three-dimensional (3D) laser microscope images of the pillar surfaces at different degrees of elongation ranging from 100 to 250%. Inserted images are the top views of each surface. All bars represent 10 μm. **e** Graph of the changes in structural parameters induced by stretching. Inserted images also indicate the line period (LP) and spike height (PP). **f** Graph of water contact angles (WCAs) and water sliding angles (WSAs). Inserted images show photographs of a 5.0 μL water droplet on the vulcanized rubber micropillar surface for each degree of elongation

Vulcanized rubber pillar arrays and wettability control

To control the surface wettability of vulcanized rubber, another type of microstructure was prepared by using a silicon mold with hexagonally arranged perpendicular micropores (ca. 5.4 μm in diameter and ca. 9.6 μm in depth) [36]. Figure 3 shows laser microscope images and graphs of the vulcanized rubber surface prepared using the silicon mold with perpendicular micropores. The vulcanized rubber surface had hexagonally arranged micropillar structures of ca. 5.3 μm in diameter and ca. 9.5 μm in height, forming a structure that mirrored the silicon mold. This arrangement was also controlled by elongation without changing the pillar structure (Fig. 3e). The WCAs on the vulcanized rubber pillar surfaces were ca. 156°, and the WSAs were ca. 15°; therefore, the WCAs and WSAs were almost constant in this elongation range (Fig. 3f). The WCA value closely matched the theoretical value of 158° obtained using the Cassie–Baxter equation with an f &value of 0.10 (only the top of the pillars were in contact with the water). Although these microstructured vulcanized rubber surfaces appeared to be merely superhydrophobic surfaces, when water droplets were dropped onto the surface, the water repellent behavior of the surfaces changed depending on the degree of elongation.

Figure 4 shows time-sequence photographs obtained by a high-speed camera during the application of 5 μL water droplets from a height of 2 cm onto the pillars of the vulcanized rubber surfaces with different degrees of elongation. In the case of 100% elongation (before stretching the rubber), the water droplet bounced off the surface, while at 150% elongation, the surface was partially wetted and the water droplet was split in two (white arrows in Fig. 4). At over 200% elongation, the microstructured rubber surfaces were wetted, and the water droplets adhered to the surface. These phenomena indicated that the wetting state was changed from a Cassie–Baxter state to a Wenzel state by transformation of the microstructure arrangement of the vulcanized rubber.

Theoretical analysis of the water behavior on vulcanized rubber pillar arrays with different degrees of elongation

We next tried to understand this phenomenon by a simple theory focusing on wettability transition and water penetration among the pillars. In this discussion, we present a semiquantitative theory in which the order of the parameters is valid, as we would like to obtain an overview of this quite variable phenomenon by comparing the magnitude relationship among factors. The driving factor is the potential

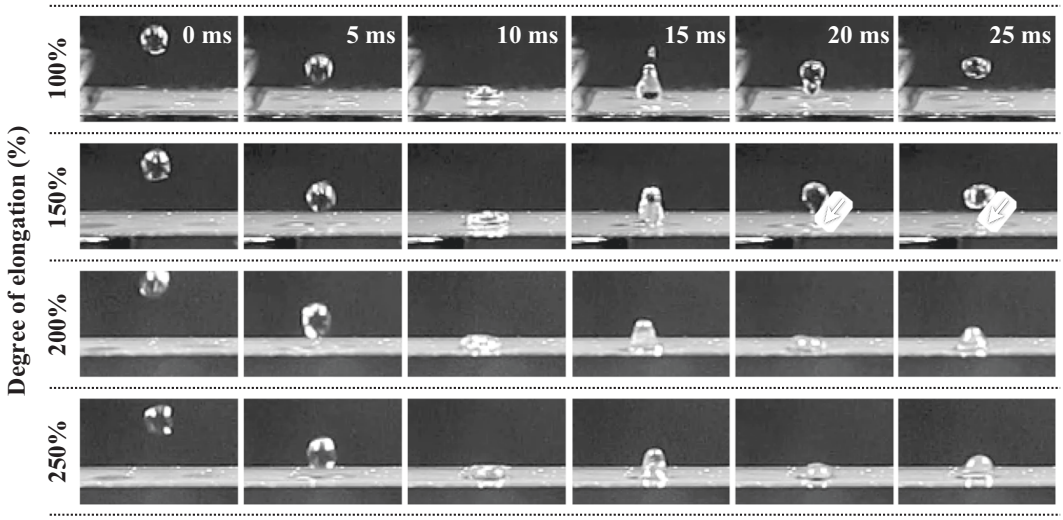

Fig. 4 Sequential photographs taken using a high-speed camera at 1200 fps during the dropping of 5.0 μL water droplets onto the vulcanized rubber micropillar surface

energy of the water droplet, and the suppression factors are excess surface energy and frictional energy, as explained below.

When a water droplet was dropped onto the microstructured vulcanized rubber surface, the water droplet was highly deformed from a sphere to a pancake- shape, so the excess surface energy of the water droplet from the sphere ΔE_{surf} appears. Furthermore, to realize a Wenzel state, water should penetrate among the hydrophobic pillar structures. In doing so, frictional energy E_{fric} is generated by the viscosity of the water. If the sum of ΔE_{surf} and E_{fric} is equal to the potential energy mgh of a water droplet, the relationship among the three energies can be described as follows:

$$mgh = \Delta E_{\mathrm{surf}} + E_{\mathrm{fric}}. \tag{4}$$

Here, mgh was ca. 1.0 μJ. When the shape of the water droplet was deformed from a sphere (5 μL, radius of 1.06 mm) to a pancake, its surface area ΔS was estimated to double, and it became 1.41×10^{-5} m^2. ΔE_{surf} is the multiple of the surface tension of water y_{water} and ΔS, and its value was calculated as ca. 1.0 μJ, which is a similar value to the potential energy of water; therefore, Eq. (4) well explains the deformation of the dropped water droplets.

Next, we focused on E_{fric} due to the water viscosity. Figure 5 shows schematic representations of E_{fric} on the patterned surface. When a water droplet was deformed to a pancake shape (Fig. 5a), the water penetrated one triangular grid hole consisting of three pillars (Fig. 5b), and frictional energy was generated (Fig. 5c). Here, considering e_{fric}, which is the frictional energy generated by the intrusion of water into one triangular grid hole, and the hole number N that came into contact with the bottom of the pancake-shaped water droplet, the energy required to transition from a Cassie–Baxter to a Wenzel state can be obtained. This energy is equal to E_{fric}:

According to previous literature reports [37], the frictional energy rate $\dot{e}_{\mathrm{fric}}$ for one hole (radius of pore: R_{pore}; depth of pore: PH) per unit time is expressed as below:

$$\dot{e}_{\mathrm{fric}} = \int\int_{0}^{R_{\mathrm{pore}}} \mathrm{d}r^2 \int_{0}^{PH} \mathrm{d}z\eta \left(\frac{\mathrm{d}v_z(r)}{\mathrm{d}r}\right)^2 = \eta v_{\mathrm{center}}^2 \times PH, \tag{5}$$

where r is $x\,y$ and η are viscosity coefficients (calculated as 10^{-3} Pa·s); R_{pore} (expressed as $2R_{\mathrm{pore}} = (PP - D)/\sin\theta_{\mathrm{pp}}$, $\mathrm{d}v_z/\mathrm{d}r$) is the gradient of the velocity of the water flowing into the hole; v_{center} is the velocity of the hole center ($mgh = (1/2)mv_{\mathrm{center}}^2$); and the gradient operates as $v_{\mathrm{center}}/R_{\mathrm{pore}}$.

On the other hand, N is given as

$$N = \frac{\Delta S}{(PP \times LP)/2}. \tag{6}$$

The combination of Eqs. (5) and (6) allows the energy-dissipation rate $\dot{E}_{\mathrm{fric}}$ due to the friction generated when water penetrates the whole gaps among pillars in contact with the bottom of a water droplet to be estimated

$$\dot{E}_{\mathrm{fric}} = \dot{e}_{\mathrm{fric}} \times N = \eta \times (2gh) \times PH \times N. \tag{7}$$

By setting the time taken for energy dissipation as τ,

$$E_{\mathrm{fric}} = \eta \times (2gh) \times PH \times N \times \tau. \tag{8}$$

Table 2 shows the calculated values for the friction energies. By setting E_{fric} for an elongation of 150%, which was the transition condition from a Cassie–Baxter to a Wenzel state, as the criterion, the friction energy for 100%

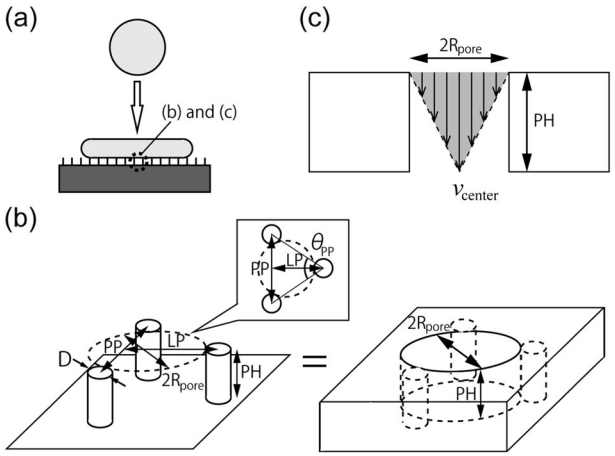

Fig. 5 Schematic representations of the friction energy on a patterned rubber surface. **a** A water droplet spreading on the surface. **b** A triangle lattice made up of three pillars (left) and its corresponding pore (right). **c** Velocity gradient of the water in the pore. Reproduced from the literature [36]

elongation was found to be 20% larger than that for 150% elongation. This result means that the penetration of water into the gaps among the vulcanized rubber micropillars was difficult because of the large friction energy and that wetting increased with an increase in the degree of elongation, in other words, with a decrease in friction energy. Moreover, because we can observe water droplet deformation by a high-speed camera with a 1 ms time resolution, τ was assumed to be 1 ms, and the E_{fric} for an elongation of 100% was calculated as 0.52 μJ. This value is half the potential energy of the water droplet (ca. 1.0 μJ); thus, friction energy could not be ignored, and a Cassie–Baxter state was maintained when the elongation was 100%. To summarize this section, by considering friction energy during the penetration of water into the microstructures, we can obtain a general understanding of the dynamic wetting behavior from a phenomenological perspective, making it possible to design wettability-controllable surfaces regulated by the degree of elongation.

Conclusion

In this report, we described a simple and easy preparation of microstructured vulcanized rubber surfaces by using silicon molds, which were processed by conventional photolithographic techniques. Furthermore, the microstructured vulcanized rubber surfaces showed novel functions generated by the surface microstructures. The spiky vulcanized rubber surface showed superhydrophobicity, with WCAs of ca. 160°. The WCAs well matched the theoretical values derived by using the Cassie–Baxter equation. The arrangement of the spikes could be rearranged from a hexagonal to a linear pattern without structural changes to the spikes by stretching, and in this case, the WCAs were constant regardless of the degree of elongation. This fact indicates that we can rearrange only the arrangement of the microstructures formed on vulcanized rubber surfaces. We also prepared vulcanized rubber micropillar surfaces to control surface wettability by stretching, and a demonstration and theoretical explanation of the water droplet behavior upon dropping onto the surface are presented. The results revealed that the surface wettability of the vulcanized micropillar array surface was dependent on the degree of elongation. When the elongation was 100%, the water droplet bounced off the surface, while water droplets could be made to adhere to the surface by increasing the elongation degree. In other words, this change in wettability represented a transition from a Cassie–Baxter to a Wenzel state. We also provided a general explanation of this quite variable phenomenon by considering the surface energy of a water droplet and the friction energy generated during water penetration into the gaps between the vulcanized micropillars.

We believe that these results can lead to the development of a new field. Generally, vulcanized rubbers are used for bulk products, such as tires, so surface microtexturing had not been considered. First, highly viscous unvulcanized rubber was not considered able to run into a micromold. However, we have demonstrated the formation of microstructured vulcanized rubber by simple hot-press molding. In this report, we showed only the functions related to wettability, but functions generated by surface microstructures not only include superwettability but also affect friction [38–40], adhesion [41], coloration [42–45], antireflection [2, 23, 46], and so on [47]. Thus, we consider that our results will stimulate the development of new fields and, in the near future, allow the production of excellent products, as vulcanized rubber is a tough, inexpensive material and is used by many people belonging to a wide variety of fields.

Table 2 Estimations of energy-dissipation rate $\dot{E}_{fric}$ and friction energy E_{fric} from a Cassie–Baxter state to a Wenzel state on the microstructured vulcanized rubber with different degrees of elongation (reproduced from the literature [36])

Degree of elongation (%)	100	150	200	250
N	1.35×10^5	1.16×10^5	9.98×10^4	8.61×10^4
$\dot{E}_{fric}$ (μJ/s)	5.24×10^2	4.44×10^2	3.93×10^2	3.29×10^2
E_{fric} (μJ)*1	0.52	0.44	0.39	0.32
Ratio	1.2	1.0	0.9	0.7

*1: The values are estimated as 1 ms

Acknowledgements This work was partially supported by the Research Program for Next Generation Young Scientists of "Dynamic

Alliance for Open Innovation Bridging Human, Environment and Materials" in "Network Joint Research Center for Materials and Devices." Preparation of the silicon micromolds was conducted at Hokkaido University and supported by the "Nanotechnology Platform" Program of MEXT, Japan.

Compliance with ethical standards

Conflict of interest The authors declare that they have no conflict of interest.

Publisher's note: Springer Nature remains neutral with regard to jurisdictional claims in published maps and institutional affiliations.

References

1. Barthlott W, Neinhuis C. Purity of the sacred lotus, or escape from contamination in biological surfaces. Planta. 1997;202:1–8. https://doi.org/10.1007/s004250050096
2. Clapham PB, Hutley MC. Reduction of lens reflection by moth eye principle. Nature. 1973;244:281–2. https://doi.org/10.1016/j.solmat.2018.05.057
3. Bhushan B. Biomimetics: lessons from nature—an overview. Philos Trans R Soc Ser A. 2009;367:1445–86. https://doi.org/10.1098/Rsta.2009.0011
4. Koch K, Bhushan B, Barthlott W. Multifunctional surface structures of plants: an inspiration for biomimetics. Prog Mater Sci. 2009;54:137–78. https://doi.org/10.1016/J.Pmatsci.2008.07.003
5. Flynn MR, Bush JWM. Underwater breathing: the mechanics of plastron respiration. J Fluid Mech. 2008;608:275–96. https://doi.org/10.1017/S0022112008002048
6. Parker AR, Lawrence CR. Water capture by a desert beetle. Nature. 2001;414:33–34.
7. Min WL, Jiang B, Jiang P. Bioinspired self-cleaning antireflection coatings. Adv Mater. 2008;20:3914. https://doi.org/10.1002/Adma.200800791.
8. Furstner R, Barthlott W, Neinhuis C, Walzel P. Wetting and self-cleaning properties of artificial superhydrophobic surfaces. Langmuir. 2005;21:956–61. https://doi.org/10.1021/La0401011
9. Budunoglu H, Yildirim A, Guler MO, Bayindir M. Highly transparent, flexible, and thermally stable superhydrophobic ORMOSIL aerogel thin films. ACS Appl Mater Interfaces. 2011;3:539–45. https://doi.org/10.1021/am101116b
10. Ghosh A, Ganguly R, Schutzius TM, Megaridis CM. Wettability patterning for high-rate, pumpless fluid transport on open, non-planar microfluidic platforms. Lab Chip. 2014;14:1538–50. https://doi.org/10.1039/c3lc51406d
11. Hirai Y, Mayama H, Matsuo Y, Shimomura M. Uphill water transport on a wettability-patterned surface: experimental and theoretical results. ACS Appl Mater Interfaces. 2017;9:15814–21. https://doi.org/10.1021/acsami.7b00806
12. Mertaniemi H, Jokinen V, Sainiemi L, Franssila S, Marmur A, Ikkala O, et al. Superhydrophobic tracks for low-friction, guided transport of water droplets. Adv Mater. 2011;23:2911–4. https://doi.org/10.1002/adma.201100461
13. Wu D, Wu S-Z, Chen Q-D, Zhang Y-L, Yao J, Yao X, et al. Curvature-driven reversible in situ switching between pinned and roll-down superhydrophobic states for water droplet transportation. Adv Mater. 2010;23:545–9. https://doi.org/10.1002/adma.201001688
14. Cao C, Ge M, Huang J, Li S, Deng S, Zhang S, et al. Robust fluorine-free superhydrophobic PDMS–ormosil@fabrics for highly effective self-cleaning and efficient oil–water separation. J Mater Chem A. 2016;4:12179–87. https://doi.org/10.1039/C6TA04420D
15. Gupta RK, Dunderdale GJ, England MW, Hozumi A. Oil/water separation techniques: a review of recent progresses and future directions. J Mater Chem A. 2017;5:16025–58. https://doi.org/10.1039/C7TA02070H
16. Lee A, Moon M-W, Lim H, Kim W-D, Kim H-Y. Water harvest via dewing. Langmuir. 2012;28:10183–91. https://doi.org/10.1021/la3013987
17. Park K-C, Chhatre SS, Srinivasan S, Cohen RE, McKinley GH. Optimal design of permeable fiber network structures for fog harvesting. Langmuir. 2013;29:13269–77. https://doi.org/10.1021/la402409f
18. Wenzel RN. Surface roughness and contact angle. J Phys Colloid Chem. 1949;53:1466–7.
19. Cassie ABD. Contact angles. Discussions of the Faraday. Society. 1948;3:11–16. https://doi.org/10.1039/DF9480300011
20. Onda T, Shibuichi S, Satoh N, Tsujii K. Super-water-repellent fractal surfaces. Langmuir. 1996;12:2125–7.
21. Hosono E, Ichihara M, Zhou HS. Fabrication of MnOOH nanorods on a substrate in an oxygen bubbled solution with superhydrophobic properties. Nanotechnology 2008;19:395605. https://doi.org/10.1088/0957-4484/19/39/395605.
22. Yabu H, Hirai Y, Kojima M, Shimomura M. Simple fabrication of honeycomb- and pincushion-structured films containing thermo-responsive polymers and their surface wettability. Chem Mater. 2009;21:1787–9. https://doi.org/10.1021/Cm803476m
23. Hirai Y, Yabu H, Matsuo Y, Ijiro K, Shimomura M. Biomimetic bi-functional silicon nanospike-array structures prepared by using self-organized honeycomb templates and reactive ion etching. J Mater Chem. 2010;20:10804–8.
24. Im M, Im H, Lee J-H, Yoon J-B, Choi Y-K. A robust superhydrophobic and superoleophobic surface with inverse-trapezoidal microstructures on a large transparent flexible substrate. Soft Matter. 2010;6:1401–4. https://doi.org/10.1039/B925970H
25. Xia F, Jiang L. Bio-inspired, smart, multiscale interfacial materials. Adv Mater. 2008;20:2842–58. https://doi.org/10.1002/Adma.200800836
26. Li X-M, Reinhoudt D, Crego-Calama M. What do we need for a superhydrophobic surface? A review on the recent progress in the preparation of superhydrophobic surfaces. Chem Soc Rev. 2007;36:1350–68. https://doi.org/10.1039/B602486F
27. Kim M, Kim K, Lee NY, Shin K, Kim YS. A simple fabrication route to a highly transparent super-hydrophobic surface with a poly(dimethylsiloxane) coated flexible mold. Chem. Commun. 2007;2237–9. https://doi.org/10.1039/B618123F.
28. Gates BD, Xu QB, Stewart M, Ryan D, Willson CG, Whitesides GM. New approaches to nanofabrication: molding, printing, and other techniques. Chem Rev. 2005;105:1171–96. https://doi.org/10.1021/Cr030076o
29. Drelich J, Miller JD, Kumar A, Whitesides GM. Wetting characteristics of liquid-drops at heterogeneous surfaces. Colloids Surf A. 1994;93:1–13.
30. Flory PJ. Network structure and the elastic properties of vulcanized rubber. Chem Rev. 1944;35:51–75. https://doi.org/10.1021/cr60110a002
31. Ho CC, Khew MC. Surface free energy analysis of natural and modified natural rubber latex films by contact angle method. Langmuir. 2000;16:1407–14. https://doi.org/10.1021/la9816104
32. Carretero-González J, Retsos H, Verdejo R, Toki S, Hsiao BS, Giannelis EP, et al. Effect of nanoclay on natural rubber microstructure. Macromolecules. 2008;41:6763–72. https://doi.org/10.1021/ma800893x
33. Hirai Y, Tamura R, Emoto S, Shimomura M, Matsuo Y, Okamatsu T, et al. Superhydrophobic microstructure imprinted rubber

sheet by hot vulcanization press. Nippon Gomu Kyokaishi. 2017;90:277–82. https://doi.org/10.2324/gomu.90.277
34. Wu B, Kumar A, Pamarthy S. High aspect ratio silicon etch: a review. J Appl Phys. 2010;108:051101. https://doi.org/10.1063/1.3474652.
35. Wang Q, Song Y, Wang L, Xiao J. Fabrication of template with dual-scale structures based on glass wet etching and its application in hydrophobic surface preparation. IET Micro Nano Lett. 2014;9:340–4. https://doi.org/10.1049/mnl.2014.0112
36. Tamura R, Hirai Y, Mayama H, Matsuo Y, Okamatsu T, Shimomura M, et al. Stretch-induced wettability changes of the superhydrophobic microstructured vulcanized rubber surface. Vac Surf Sci. 2018;61:348–53. https://doi.org/10.1380/vss.61.348
37. Nishimura R, Hyodo K, Sawaguchi H, Yamamoto Y, Nonomura Y, Mayama H, et al. Fractal surfaces of molecular crystals mimicking lotus leaf with phototunable double roughness structures. J Am Chem Soc. 2016;138:10299–303. https://doi.org/10.1021/jacs.6b05562
38. Wang X, Kato K, Adachi K, Aizawa K. Loads carrying capacity map for the surface texture design of SiC thrust bearing sliding in water. Tribology Int. 2003;36:189–97. https://doi.org/10.1016/S0301-679X(02)00145-7
39. Varenberg M, Gorb SN. Hexagonal surface micropattern for dry and wet friction. Adv Mater. 2009;21:483–6. https://doi.org/10.1002/Adma.200802734
40. Suzuki K, Hirai Y, Ohzono T. Oscillating friction on shape-tunable wrinkles. ACS Appl Mater Interfaces. 2014;6:10121–31. https://doi.org/10.1021/am5010738
41. Autumn K, Liang YA, Hsieh ST, Zesch W, Chan WP, Kenny TW. et al. Adhesive force of a single gecko foot-hair. Nature. 2000;405:681. https://doi.org/10.1038/35015073.
42. Kinoshita S, Yoshioka S, Fujii Y, Okamoto N. Photophysics of structural color in the morpho butterflies. Forma. 2002;17:103.
43. Sato O, Kubo S, Gu Z-Z. Structural color films with lotus effects, superhydrophilicity, and tunable stop-bands. Acc Chem Res. 2009;42:1–10. https://doi.org/10.1021/ar700197v
44. Saito A. Material design and structural color inspired by biomimetic approach. Sci Technol Adv Mater. 2011;12:064709. https://doi.org/10.1088/1468-6996/12/6/11661028.
45. Yabu H, Nakanishi T, Hirai Y, Shimomura M. Black thin layers generate strong structural colors: a biomimetic approach for creating one-dimensional (1D) photonic crystals. J Mater Chem. 2011;21:15154–6. https://doi.org/10.1039/C1jm13094c
46. Huang YF, Chattopadhyay S, Jen YJ, Peng CY, Liu TA, Hsu YK, et al. Improved broadband and quasi-omnidirectional anti-reflection properties with biomimetic silicon nanostructures. Nat Nanotechnol. 2007;2:770–4. https://doi.org/10.1038/Nnano.2007.389
47. Ball P. Engineering Shark skin and other solutions. Nature. 1999;400:507. https://doi.org/10.1038/22883.

Yuji Hirai received his B.Sc. and M.Sc. degrees from the Hokkaido University. He obtained his Ph.D. under the supervision of Professor Dr Masatsugu Shimomura from the Tohoku University in 2010, and he started his research career in IMRAM, Tohoku university as an assistant professor. In 2013, He became lecturer of Chitose institute of science and technology. His research interests are biomimetic engineering, tribology, surface science, bottom up technology, self-organization, self-assembly, colloidal crystal, nanotechnology, polymer chemistry, organic/inorganic hybrid materials, metal nano structures, and applications of nano and micro structures. He received the Award for Encouragement of Research in Polymer Science; The Society of Polymer Science, Japan (2018).

Hiroyuki Mayama is an associate professor in Department of Chemistry at Asahikawa Medical University, Asahikawa in Japan. He received his Ph.D. in Engineering from Hokkaido University in 1999 in the field of superconductivity. From 1999 to 2003, he was a postdoctoral fellow in Kyoto University and then studied first-order phase transition of stiff polymer chains and nonlinear science. From 2003 to 2012, he was an assistant professor in Research Institute for Electronic Science at Hokkaido University and then studied fractal science and wetting phenomena. He moved to Department of Chemistry at Asahikawa Medical University. His research interests cover wetting phenomena, polymer physics, nonlinear science, fractal and biomimetics.

Riku Tamura received his B. and M. degrees under the supervision of Professor Dr Masatsugu Shimomura from the Chitose Institute of Science and Technology. His research field was preparations of novel superhydrophobic surfaces, especially, he mainly used vulcanized microstructured rubbers. He received the poster award for Young Researchers of the 67th Divisional Meeting of Division of Colloid and Surface Chemistry.

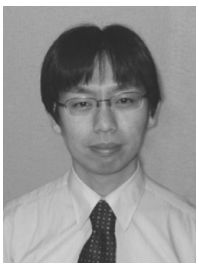

Yasutaka Matsuo is a Professor of Research Institute for Electronic Science (RIES) in Hokkaido University, Sapporo Japan. He received his B.Eng., M.Eng. from Osaka University and Ph.D. from Hokkaido University. He became a postdoctoral fellow at the Japan Science and Technology (JST) agency PRESTO project by Prof. Ijiro in 2001. He was an assistant professor in RIES, Hokkaido University from 2004 to 2009 and he was an associate professor in RIES, Hokkaido University from 2010 to 2018. From 2018, he became professor in RIES, Hokkaido University. He manages Promotion Office for Nanotechnology Collaboration. He is also participating in Nanotechnology Platform program by MEXT at Hokkaido University from2012. His research currently focuses on the functional surface fabricated by nanotechnology.

Takahiro Okamatsu is a general manager of Okamatsu Laboratory in Research & Development center of THE YOKOHAMA RUBBER CO., LTD (YRC), Kanagawa in Japan. After getting his B.Eng and M.Eng from Doshisha University, He started working for Kanebo LTD as a research chemist from 1991. He received his Ph.D in Applied Chemistry from Kansai University in 2001. He joined in YRC at 2004 and became a senior engineer at the next year. He has been appointed as a general manager in the laboratory since 2010. His major interests are adhesion phenomena, surface and interphase of rubber-based composite materials and science and technology of the colloids including organic/inorganic nano-particles and polymer emulsions. He received the Outstanding Paper Award from the adhesion society of Japan in 2007.

Toshihiko Arita completed his doctorate in physical chemistry at Kyoto University in 2003. After his graduation of Kyoto University, he started physical chemistry of polymer materials in Georg-August-Universität Göttingen, Germany as a post doctorate fellow. He also spent his days in Institute for Chemical Research (ICR) of Kyoto University as a post doctoral fellow. He currently belongs to Institute of Multidisciplinary Research for Advanced Materials (IMRAM) of Tohoku University as an Assistant Professor from 2007. He has been studying polymer-surface-functionalized fillers produced by Polymerization with Particles (PwP) technique invented by himself. He recently founded an University venture company, FillerBank Limited, in 2017 in order to accelerate and spread application of cellulose nanocrystal (CNC) powder.

Masatsugu Shimomura After graduating from Kyushu University, Masatsugu Shimomura engaged in the field of biomimetic chemistry as an assistant professor of Prof. Toyoki Kunitake's laboratory. He developed the research of polymeric Langmuir-Blodgett films at Tokyo University of Agriculture and Technology as an associate professor, and moved to Hokkaido University for starting a new laboratory of the bottom-up nanotechnology based on self-organization and biomimetics. Self-organized honeycomb-patterned polymer films are newly developed by collaboration with many industrial companies and the RIKEN institute where he held concurrently post of the principle investigator. After moving to Tohoku University, he organized a national research project on Engineering Neo-Biomimetics, and started an educational program on biomimetics at Chitose Institute of Science and Technology. He is a Professor Emeritus of Hokkaido University and Tohoku University.